A Three-Phase High-Frequency Semicontrolled Rectifier for PM WECS

Demercil S. Oliveira, Jr., Mônica M. Reis, Carlos E. A. Silva, Luiz H. S. Colado Barreto, *Member, IEEE*, Fernando L. M. Antunes, *Member, IEEE*, and Bruno L. Soares

***Abstract*—This paper proposes the use of a three-phase high-frequency semicontrolled rectifier for wind energy conversion systems based on permanent magnet generators. The main advantages of the topology are: simplicity, since all active switches are connected to a common point, robustness, as short-circuit through a leg is not possible, and high efficiency due to reduced number of elements. As a disadvantage, higher but acceptable total harmonic distortion of the generator currents results. The complete operation of the converter and theoretical analysis are presented. Additionally, a single-phase pulsewidth modulation inverter is also employed in the grid connection. Experimental results on 5-kW prototype are presented and discussed.**

***Index Terms*—Grid-connected systems, power factor correction, three-phase pulsewidth modulation (PWM) rectifiers, wind energy conversion systems (WECSs).**

I. Introduction

ACCORDING to the U.S. Department of Energy, as mentioned in the International Energy Outlook 2006 (IEO) report of Energy Information Administration (EIA), the global consumption of energy will grow at an annual average rate of 2% between 2003 and 2030. The forecast for the growth of demand for energy, specifically in the electric form, is even higher, i.e., 2.7% per year [1].

Either for ambient, strategical, or geographic issues, the generation of electric energy from wind energy systems has grown quickly, changing from a global installed power of 4.8 GW in 1995 to 58 GW in 2005, at annual average growth of 24% [2]. Considering the current estimations of increase in the demand for electric energy generation in the next few years, one concludes that the generation of electric energy from wind systems tends to continue [3], [4]. As the electrical power available from a wind energy conversion system (WECS) based on permanent magnet (PM) generators cannot be delivered directly to the grid, power electronics plays a decisive role in overcoming this limitation [4].

Although small WECs have been used in remote locations where conventional grid is not available, recently, small WECS are being considered to be used in parallel with the local grid. Then, at low wind speeds, the WECS feeds partially the loads and at high wind speeds, the exceeding energy is injected to the grid. This leads to the reduction of the utility bill with consequent amortization of the initial investment cost. Within this context, cost and efficiency of small WECS are essential to the economical viability and practical implementation.

Then, this paper proposes a grid-connected, variable-speed WECS feasible to low-power applications. Robustness, simplicity, low cost, and high efficiency are inherent characteristics because few semiconductor elements are used. The operating principle, theoretical analysis, as well as experimental results obtained from a 5-kW prototype are presented and discussed.

Manuscript received January 19, 2009; revised March 26, 2009 and September 11, 2009. Current version published April 2, 2010. This work was supported by Centrais Elétricas Brasileiras SA, Enersud Industry and Energy Solutions Ltda, Financiadora de Estudos e Projetos, and Fundação Cearense de Amparo à Pesquisa. Recommended for publication by Associate Editor Z. Chen.

The authors are with the Group of Power Processing and Control, Federal University of Ceará, Fortaleza 60020-181, Brazil (e-mail: demercil@dee.ufc.br; demercil@yahoo.com.br; mon_m_r@hotmail.com; carloselmano@gmail.com; lbarreto@dee.ufc.br; fantunes@dee.ufc.br; brunolucassoares@gmail.com).

Digital Object Identifier 10.1109/TPEL.2009.2034263

II. Wind Energy Conversion Systems

The wind turbine basic principle is to convert the linear motion of the wind into rotational energy, which is used to drive an electrical generator, allowing the kinetic energy of the wind to be converted to electric power. The captured power of the wind (P_v) for a wind turbine is given by [4]

$$P_v = \frac{1}{2}\rho_a A_v u^3 \tag{1}$$

where "ρ_a" is the wind density, "u" is the wind speed, and "A_v" is the area swept by the turbine. The mechanical power (P_m) generated by the wind turbine from captured power of the wind depends on the power coefficient (C_p) of the wind turbine, as shown in the following:

$$P_m = C_p(\lambda, \beta)\, P_v \tag{2}$$

where C_p is a function of tip-speed ratio λ and pitch angle β, which is developed satisfactorily in [3].

Any WECS is basically composed of three parts: the wind turbine, electrical power generator, and electronic power processing system. Horizontal-axis wind turbines (HAWTs) with two and three blades are the ones that allow the best exploitation of the available wind energy [4]. Three-bladed HAWTs are more commonly used than two-bladed ones because they are less susceptible to the tower shadow effect and achieves higher power coefficient.

Fig. 1 shows that the maximum extraction of the wind energy is achieved by keeping parameter λ constant; therefore, the rotational speed of the turbine is supposed to vary with the wind speed, since variable-speed WECSs provide better energy extraction. Then, fixed-speed WECSs, as that one directly connected to the power grid or the one proposed in [6], imply bigger wind turbine blades.

The possibility to control the frequency and amplitude of the generated voltage through the excitation, independently of the

0885-8993/$26.00 © 2010 IEEE

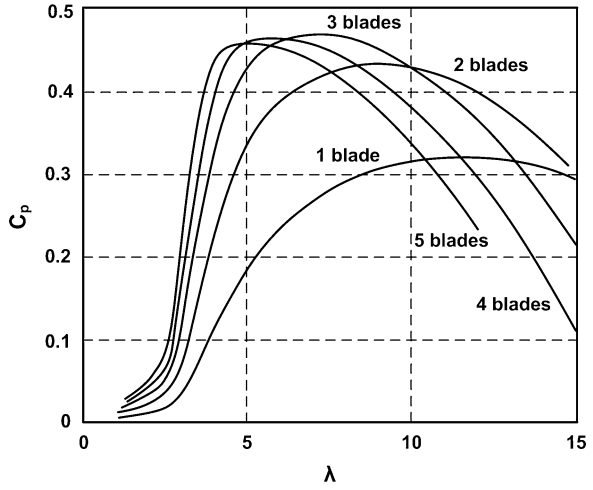

Fig. 1. Power coefficient versus tip-speed ratio curves for HAWTs [4].

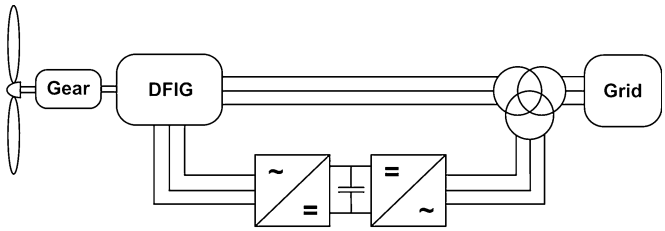

Fig. 2. Variable-speed WECS directly connected to the grid based on DFIG.

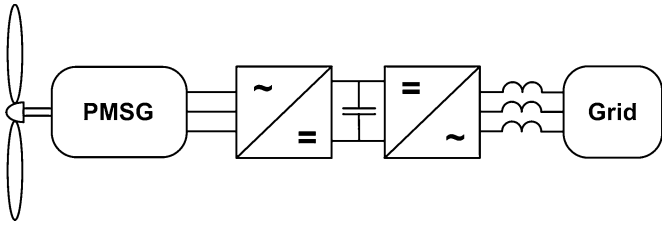

Fig. 3. Variable-speed WECS connected to the grid based on PMSG.

speed rotation, has made the doubly fed induction generator (DFIG) the main choice in variable-speed WECSs of great size directly connected to grid (see Fig. 2) [8], [9].

The WECS in Fig. 2 allows the processing of high power levels, since the power converter processes only about 30% of the rated power [10]. On the other hand, the reduced number of poles of the DFIG demands the use of gearbox between the wind turbine and the generator, implying increased weight, size, and maintenance need, reducing its efficiency and reliability [8].

An alternative to the DFIG is the PM-synchronous generator (PMSG), which can be designed with higher number of poles to avoid the use of gearbox. Being a synchronous generator, all the generated power must be conditioned through a power converter, before it can be used (see Fig. 3), restricting the power processed by this type of WECS.

The PMSG presents some advantages when compared with the DFIG [11], [12], which are as follows:

1) it does not require any external excitation current, which reduces losses;

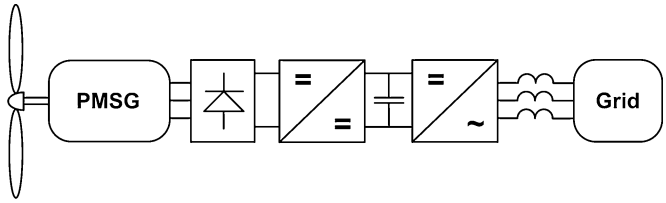

Fig. 4. WECS with power factor correction using intermediate dc–dc stage.

2) light weight;
3) small size;
4) high reliability;
5) low maintenance;
6) high efficiency;
7) smaller wind turbine blade.

Although the main disadvantage of the PMSG is the high cost of the PM material and power converter, the absence of the gearbox makes the PMSG the main choice for small WECSs (<100 kW).

A. Power Processing Topologies Applied to PMSG

In Fig. 3, the rectifier stage can be based on the Graetz rectifier that produces variable voltage in the dc link. Then, the inverter stage operates with poor device utilization, since it operates with low modulation ratio in higher power operation [12]. In order to supply a constant-voltage dc link of the inverter stage, a dc–dc stage is introduced between the conventional rectifier and the output stage [13], as shown in Fig. 4.

However, the rectifier stage of the power converter used in systems, such as that in Fig. 4, causes high distortion of the current and voltage of PMSGs, implying several undesirable effects to the generator, such as [15], which are as follows:

1) increased heating due to iron and copper losses at the harmonic frequencies;
2) reduction in machine efficiency;
3) loss of the torque production;
4) increased audible noise emission;
5) eventual occurrence of mechanical oscillations.

In order to avoid these problems, it is interesting to use systems capable of emulating resistive loads for the PMSG, resulting in low total harmonic distortion (THD).

In grid-connected applications, a step-up dc–dc converter, with current–source input characteristic, can be used in the WECS of Fig. 4. The simplicity of control, the reduced number of components, and the predominant need to increase the generated voltage make the boost converter the main choice [16]–[21] in this WECS, as shown in Fig. 5.

Fig. 5 shows that in the rectifier stage the instantaneous conduction losses are caused by the voltage across the diodes (about $2V_t$, where V_t is the voltage drop in one rectifier diode). Also, the instantaneous conduction losses in the dc–dc stage are caused by the conduction of the boost diode D_b or switch S_b. Then, one can see that there are always three semiconductors in the current path from the generator side to the dc-link side, which reduces the efficiency of this topology. Also, power factor correction is achieved only in discontinuous-conduction mode. Then, this structure becomes feasible for small WECSs.

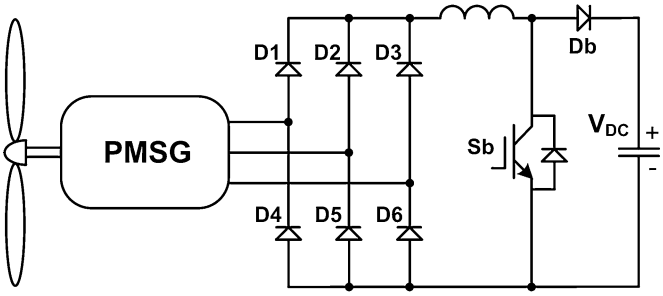

Fig. 5. WECS with intermediate boost converter.

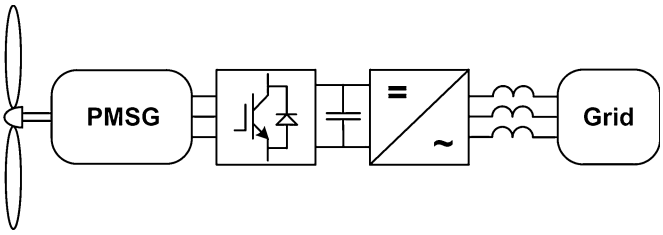

Fig. 6. WECS with power factor correction using PWM rectifier.

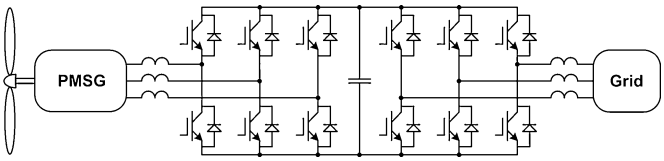

Fig. 7. WECS with back-to-back converter.

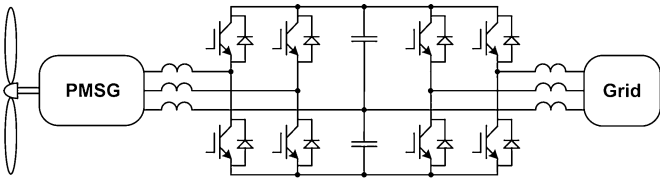

Fig. 8. WECS with modified back-to-back converter.

Another option to achieve high power factor in the generator side is to use a pulsewidth modulation (PWM) rectifier in the WECS, as shown in Fig. 6.

The traditional topology applied in high-power WECS is shown in Fig. 7 [9] and uses the back-to-back converter [22], [23]. In the rectifier stage of this structure, the currents can be modulated in both half cycles. However, the half-bridge connected switches demand the use of bootstrap-integrated circuits, and the occurrence of eventual short-circuits through the leg is possible.

Fig. 8 shows a WECS that uses a variation of the back-to-back converter [24], proposed in [25]. Only four semiconductors are used in the rectifier stage of this topology. Moreover, the small number of components and voltage balance across the dc-link capacitors limit the use of modified modulation techniques for the optimization of losses [26], [27].

III. Proposed WECS

The WECS in Fig. 9 is composed of a PMSG rated at 5 kVA, being connected to a power factor correction semicontrolled rectifier. The latter structure uses three insulated-gate bipolar transistors (IGBTs) and three diodes [29]. The dc–ac stage of the wind system is a single-phase full-bridge topology with unipolar modulation. The rms current injected into the grid provides regulation of the dc-link voltage.

The main advantages of the proposed WECS when compared to standard WECSs are as follows.

1) All switches are connected to the same reference in rectifier stage, simplifying the command circuit.
2) There are no switches in series in the rectifier stage, discharging the possibility of short-circuit through a leg.
3) The small number of power stages increases efficiency when compared to the topology shown in Fig. 5.

The main disadvantage of the considered WECS is the higher harmonic content when compared to the traditional PWM back-to-back topology, since only the positive half-cycle can be modulated.

A. Rectifier Operation

The rectifier stage in Fig. 10 operates as a boost converter. When one of the switches S_1, S_2, or S_3 is turned on, the current flows through it and the current through the respective inductor will increase, while the respective diode D_1, D_2, or D_3 is reverse biased. When switch S_1, S_2, or S_3 is turned off, the respective diode D_1, D_2, or D_3 is forward biased, the current will flow through it and the energy will be transferred to the dc link.

The input currents I_a, I_b, and I_c can assume three states: null (0), positive (+), or negative (−), resulting in 27 combinations. However, only 12 combinations are physically pertinent, which are shown in Table I.

Since a semicontrolled rectifier is used, combinations 10, 11, and 12 cannot be implemented. Therefore, the negative half-cycles of I_a, I_b, and I_c cannot be modulated, resulting in the theoretical waveforms shown in Fig. 11.

Fig. 11 shows that a complete period of the currents I_a, I_b, and I_c can be divided in nine sectors. Following the same criterion, similar sectors can be subdivided in three groups: [1, 4, and 7], [2, 5, and 8], and [3, 6, and 9]. Therefore, the description of sectors 1– 3 is enough for the comprehension of the remaining ones.

1) Sector 1: In this sector, currents I_a and I_b are positive, and current I_c is negative. Thus, in this sector, the rectifier has 2 DOF, associated to the states of switches S_1 and S_2, resulting in the four possible topological states, as shown in Fig. 12.

The corresponding equivalent circuits for these topological states are shown in Fig. 13.

2) Sector 2: In this sector, current I_a is positive, current I_b is nearly null, and current I_c is negative. Therefore, in this sector, the rectifier has only one degree of freedom, which is associated to the state of the switch S_1, resulting in the topological states of Fig. 14. The corresponding equivalent circuits are given in Fig. 15.

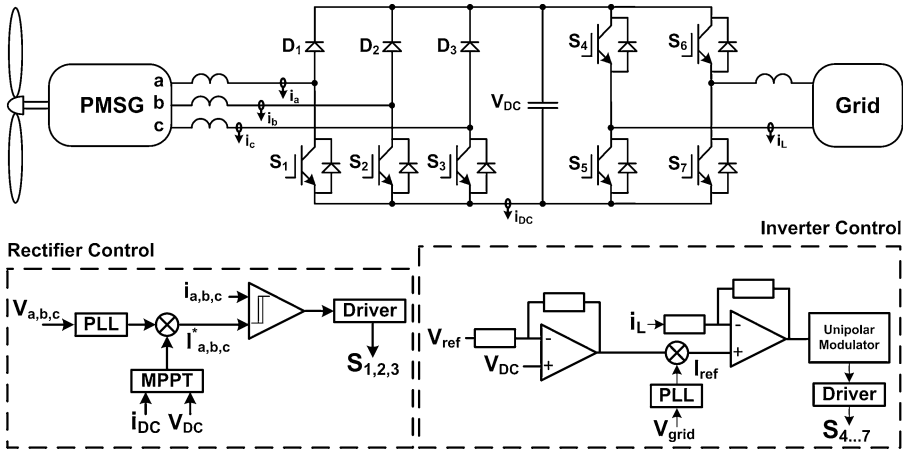

Fig. 9. Schematic diagram of the proposed WECS.

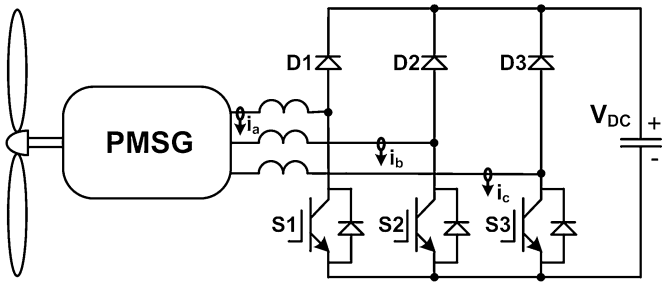

Fig. 10 Schematic diagram of the proposed rectifier stage.

TABLE I
POSSIBLE COMBINATIONS FOR THE INPUT CURRENTS

	1	2	3	4	5	6	7	8	9	10	11	12
I_A	+	+	+	+	0	-	-	-	0	+	-	-
I_B	+	0	-	-	-	0	+	+	+	-	+	-
I_C	-	-	0	+	+	+	+	0	-	-	-	+

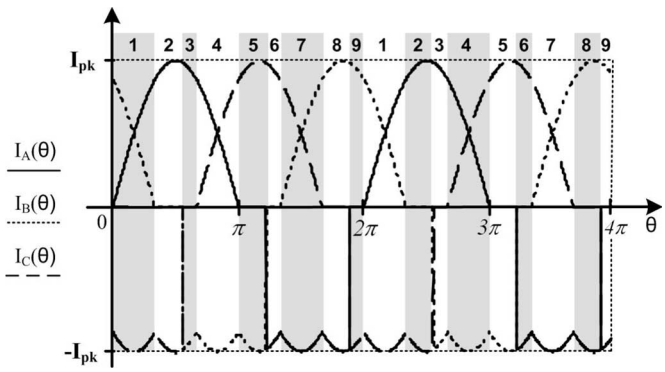

Fig. 11. Theoretical waveforms of currents I_a, I_b, and I_c.

3) Sector 3: In this sector, current I_a is positive, current I_b is negative, and current I_c is nearly null. Thus, in this sector, the rectifier has only one degree of freedom, which is also associated to the state of switch S_1, resulting in the topological states of Fig. 16. The corresponding equivalent circuits are given in Fig. 17.

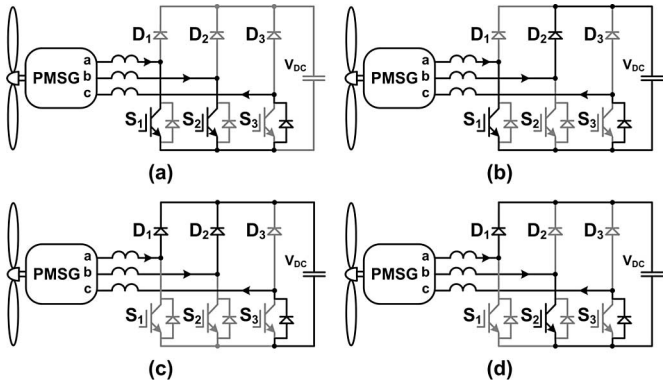

Fig. 12. Topological states associated to sector 1.

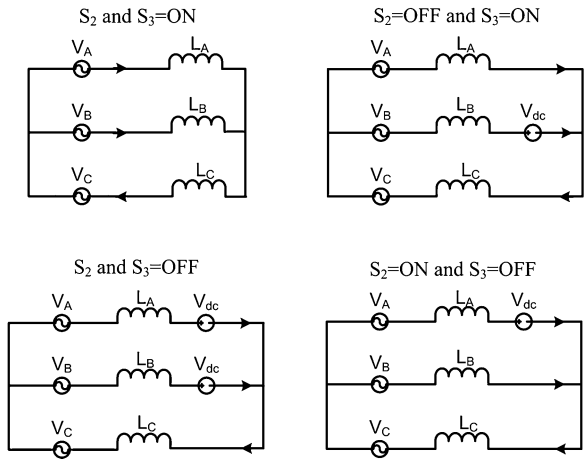

Fig. 13. Equivalent circuits associated to sector 1.

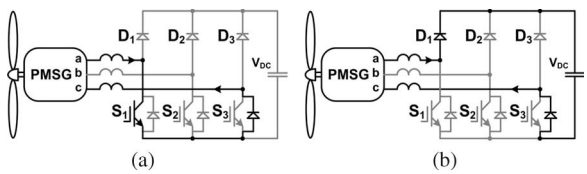

Fig. 14. Topological states associated to sector 2.

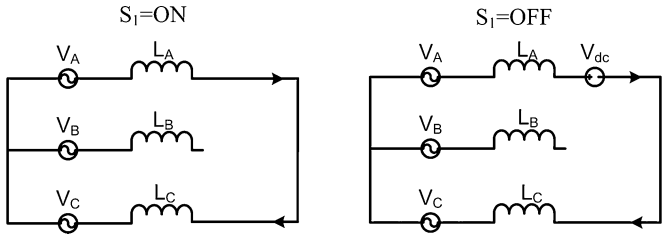

Fig. 15. Equivalent circuits associated to sector 2.

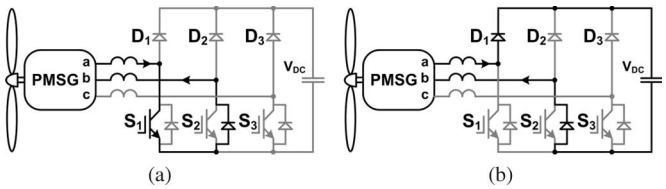

Fig. 16. Topological states associated to sector 3.

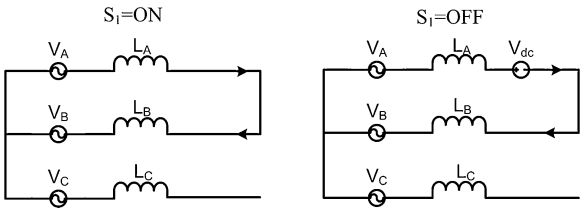

Fig. 17. Equivalent circuits associated to the sector 3.

TABLE II
DUTY-CYCLE BEHAVIOR

Sector	Duty Cycle Behavior
1	$D_{1A}(\omega t) = 1 - M_r\sqrt{3}\sin(\omega t + 30^o) + \beta\sqrt{3}\cos(\omega t + 30^o)$
2	$D_{2A}(\omega t) = 1 - M_r\sqrt{3}\sin(\omega t + 30^o) + 2\beta\cos(\omega t)$
3	$D_{1A}(\omega t) = 1 - M_r\sqrt{3}\sin(\omega t) + 2\beta\cos(\omega t)$
4	$D_{4A}(\omega t) = 1 - M_r\sqrt{3}\sin(\omega t - 30^o) + \beta\sqrt{3}\cos(\omega t - 30^o)$

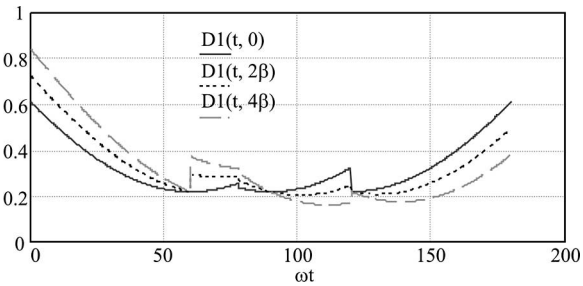

Fig. 18. Duty-cycle behavior of switch S_1 to obtain reduced THD.

The fourth sector is analogous to the first one and the subsequent stages follow the same behavior described before. From the obtained equivalent circuits, the equations presented in Table II can be obtained, which describe the duty-cycle behavior to obtain lower THD. It can be seen from Fig. 18 that there are the same discontinuities in the duty-cycle values during the transitions among the sectors. This discontinuity implies fast controller response in order to achieve low-current THD.

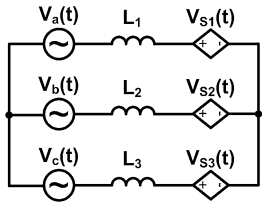

Fig. 19. Equivalent circuit of the rectifier seen from the input side.

B. Rectifier Dynamic Model

The rectifier can be modeled by the equivalent circuit in Fig. 19, where $V_a(t)$, $V_b(t)$, and $V_c(t)$ are the PMSG-generated instantaneous voltages, L_1, L_2, and L_3 are the respective boost inductances, and$V_{S1}(t)$, $V_{S2}(t)$, and $V_{S3}(t)$ are the instantaneous average voltages seen by each phase, as given by

$$\begin{bmatrix} V_{S1}(t) \\ V_{S2}(t) \\ V_{S3}(t) \end{bmatrix} = \begin{bmatrix} (1 - D_{S1}(t)) \\ (1 - D_{S2}(t)) \\ (1 - D_{S3}(t)) \end{bmatrix} V_{dc} \tag{3}$$

where $D_{S1}(t)$, $D_{S2}(t)$, and $D_{S3}(t)$ are instantaneous functions of the effective duty cycle of switches S_1, S_2, and S_3, respectively. Considering the PMSG-generated voltages balanced and the absence of the neutral conductor, and applying the Kirchhoff's law to the circuit in Fig. 19, the dynamic model if the rectifier is obtained and given in matrix form by

$$\begin{bmatrix} I_a(s) \\ I_b(s) \\ I_c(s) \end{bmatrix} = \frac{1}{3Ls} \begin{bmatrix} -2 & 1 & 1 \\ 1 & -2 & 1 \\ 1 & 1 & -2 \end{bmatrix} \begin{bmatrix} V_{S1}(s) \\ V_{S2}(s) \\ V_{S3}(s) \end{bmatrix}. \tag{4}$$

C. Rectifier Control

Through simulation studies, it was verified that constant-frequency PWM controllers tend to increase the current THD due to the discontinuities shown in Fig. 18. Then, the rectifier control system uses the principle of hysteresis control. The input currents through each phase (I_a, I_b, and I_c) are measured and compared to the respective reference currents (I^*_a, I^*_b, and I^*_c). The reference current shapes are obtained from the respective input voltages, and their peak values are given by a maximum power point tracking (MPPT) algorithm. The employed MPPT algorithm consists in measuring the frequency of the generator voltage through a phase-locked loop (PLL) circuit. Then, the current peak values are obtained from a preprogrammed table.

Switching operation occurs when the current limits are reached, as shown in Fig. 20. With this technique, the obtained line currents achieve low THD with a simple control circuitry.

The main disadvantage of the hysteresis control is the variable switching frequency. However, switching frequency can be maintained within acceptable range by adjusting the hysteresis band.

D. Loss Estimation

In order to estimate the efficiency of the proposed converter, a loss analysis was performed, considering the developed

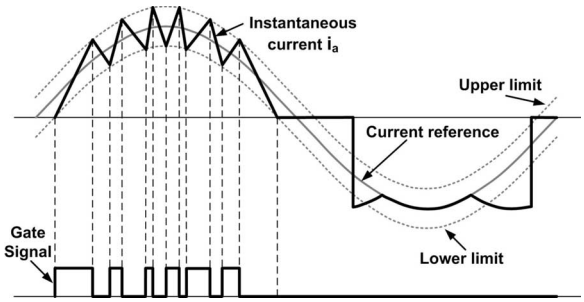

Fig. 20. Switching pattern of the hysteresis control applied to the rectifier stage.

TABLE III
SEMICONDUCTORS AND MAIN PARAMETERS

Parameter	Especification	Parameter	Especification
S_1, S_2, S_3	IRGP50B60PD1	S_b	IRGP50B60PD1
D_1, D_2, D_3	HFA15PB60	D_b	HFA25TB60
V_{in}	55V – 220 V	D_1,…,D_6	12F40
V_{dc}	400 V	V_{dc}	400 V
P_0	375 W-6k W		

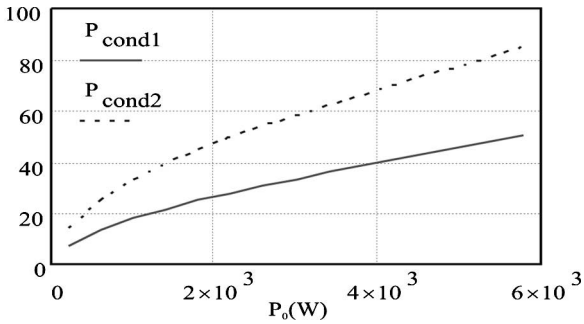

Fig. 21. Estimated switching losses for the proposed rectifier stage (P_{sw1}) and for the conventional rectifier associated with a boost converter (P_{sw2}).

equations, the semiconductors, and parameters given in Table III and the respective datasheets.

Fig. 21 presents the switching losses in the semiconductors for the proposed topology depicted in Fig. 10 (P_{sw1}) and for the conventional topology shown in Fig. 5 (P_{sw2}). It can be seen that the total switching losses are near the same over the entire power range. In Fig. 22, the calculated conduction losses through the semiconductors for the proposed topology (P_{cond1}) and the conventional topology (P_{cond2}) are shown. As it can be seen, the proposed topology has less conduction losses due to the fewer number of semiconductors. Fig. 23 compares the estimated efficiency of the proposed rectifier stage (η_1) with the conventional rectifier stage associated with the boost stage (η_2). It can be seen that the proposed rectifier has improved efficiency over the entire power range, mainly at low and medium power levels, which is an interesting advantage in WECS applications.

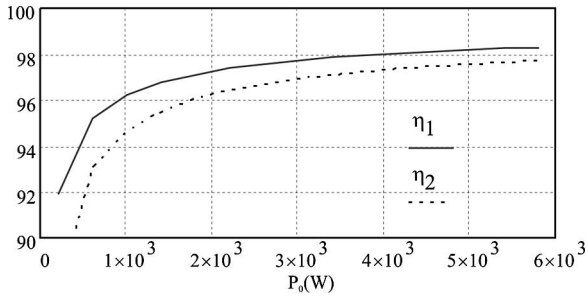

Fig. 22. Estimated conduction losses for the proposed rectifier stage (P_{cond1}) and for the conventional rectifier associated with a boost converter (P_{cond2}).

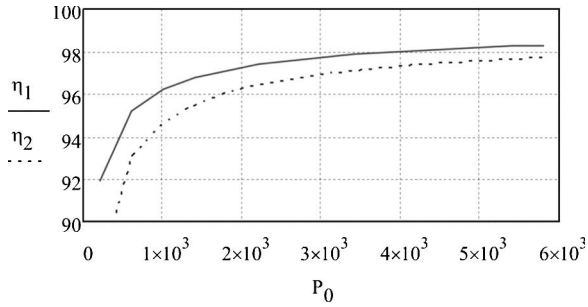

Fig. 23. Estimated efficiencies for the proposed rectifier stage (η_1) and for the conventional rectifier associated with a boost converter (η_2).

TABLE IV
RECTIFIER SPECIFICATIONS AND PARAMETERS

Parameter	Specification
Rms input voltage range	95 V – 213 V
Grid frequency range	60 Hz
Output voltage	400 V
Switching frequency range	10 – 25 kHz
Input inductors	1 mH
Input power	0 - 5,5 kW

TABLE V
INVERTER SPECIFICATIONS AND PARAMETERS

Parameter	Specification
Dc link voltage	400 V
Grid voltage	220 V
Grid frequency	60 Hz
Output inductor	1.5 mH
Switching frequency	30 kHz
Output power	0 – 5 kW

IV. EXPERIMENTAL RESULTS

The proposed rectifier prototype was built and tested. The specifications and parameters used in the prototype are shown in Tables IV and V.

Fig. 24 shows the current through phase "a," and the respective phase voltage at rated power. Power factor is equal to 0.982 and the THD is about 18%. In a conventional Graetz rectifier, typical power factor and THD are about 0.94% and 35%,

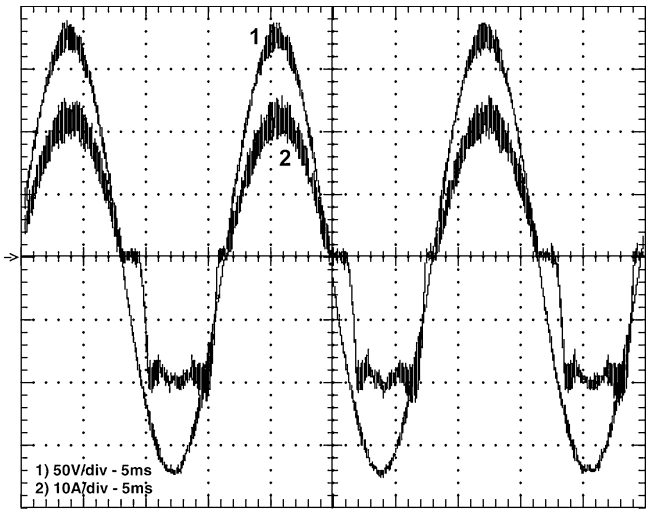

Fig. 24. Rectifier current (10 A/div, 5 ms) and voltage (50 V/div, 5 ms) waveform of phase "a".

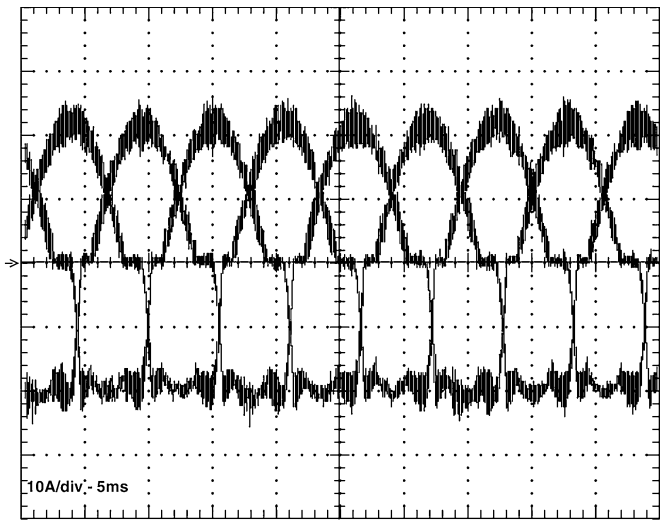

Fig. 25. Rectifier current waveform for input line voltage of 213 V_{rms} (10 A/div, 5 ms).

respectively. This improvement in the power factor represents a reduction of about 10% in the generator conduction losses.

Fig. 25 presents the three line currents for an rms input voltage equal to 213 V and rated power. A good equilibrium among the currents can be seen.

Fig. 26 shows the harmonic spectrum of the input current at rated power, where the second-, fourth-, and fifth-order components are the most relevant.

Considering that in the proposed converter the harmonic spectrum is more concentrated in low-order harmonics than in the Graetz rectifier, and also that the THD for the proposed rectifier is lower, additional gain due to the skin effect losses reduction is achieved. While the winding resistances tend to be smaller due to the reduced temperature of the generator, conduction losses are even more reduced.

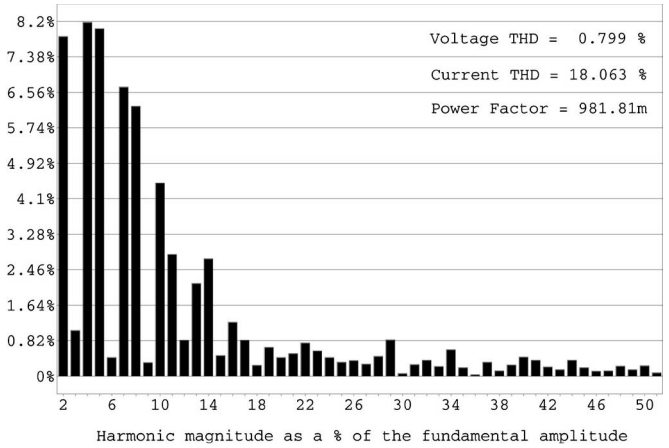

Fig. 26. Harmonic spectrum of the input current ($V_{in} = 213\ V_{rms}$ and $P_{out} = 5$ kW).

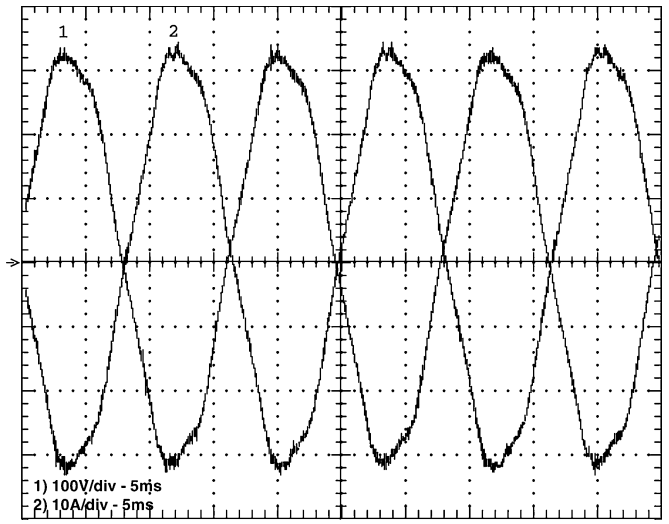

Fig. 27. Grid voltage (1–100 V/div, 5 ms) and inverter–grid current (2–10 A/div, 5 ms) waveforms.

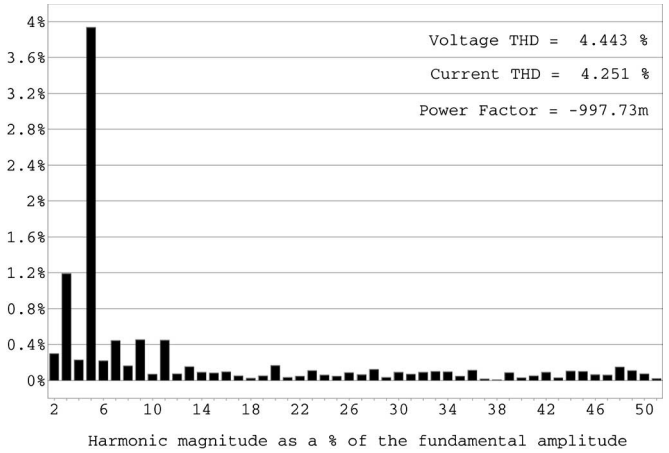

Fig. 28. Harmonic spectrum of the grid-injected current.

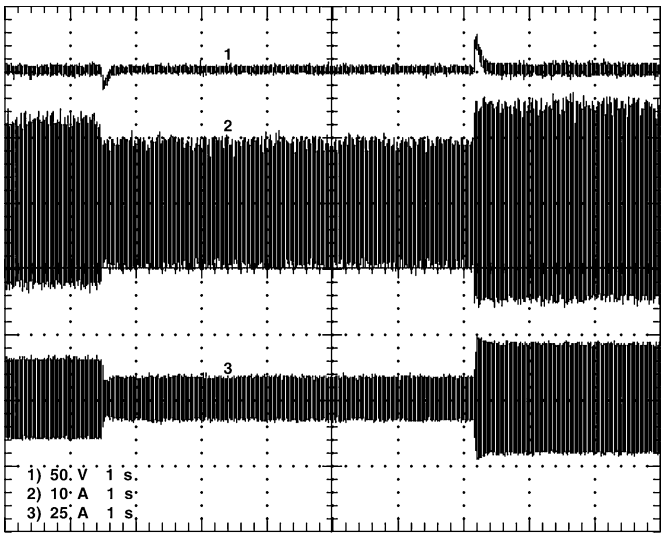

Fig. 29. DC-link voltage (1–50 V/div, 1 s), input rectifier current (2–10 A/div, 1 s), and grid-injected current waveform (3–25 A/div, 1 s).

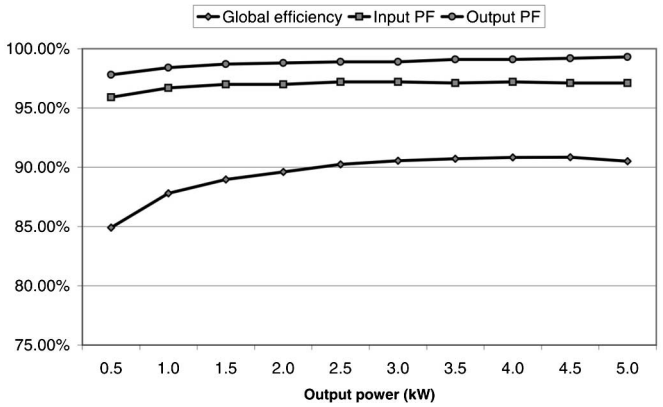

Fig. 30. Efficiency versus output power, input power factor versus output power, and output power factor versus output power.

Fig. 27 shows the inverter–grid current and the grid voltage for a power factor around 0.998. The THD of the grid-injected current is about 4.25%. The third and the fifth harmonics are the most relevant components, as shown in Fig. 28.

Fig. 29 shows the dynamic response for step changes in the rectifier input voltage from 95 to 70 V_{rms} and from 70 to 111 V_{rms}. The response is slow, in order to keep the THD of the grid-injected current low and achieve satisfactory voltage regulation. Fig. 30 shows the measured efficiencies. This demonstrates the expected improvement when compared with similar works.

V. Conclusion

A WECS feasible for micro and small turbines has been presented in this paper. The main advantages of the proposed system when compared to a conventional WECS are the use of switches with the source connected to the same point, robustness due to the absence of controlled switches in the same leg, and high efficiency due to reduced number of components.

To control the rectifier, the principle of hysteresis control is employed. With this technique, the obtained line currents have acceptable THD with a simple control circuit (<20%). The inverter stage is based on one-phase full-bridge inverter using symmetrical unipolar modulation.

The loss analysis demonstrated an expected losses reduction in the ac–dc stage of about 0.5% when compared to the traditional Graetz rectifier associated with a boost converter, due to a reduction in the conduction losses. This reduction occurs for the whole power range, which is an interesting characteristic for WECS applications. Considering that in the proposed converter, the harmonic spectrum is more concentrated in low-order harmonics than in the Graetz rectifier, and also that the obtained THD in this case is lower, additional gain due to the skin-effect losses reduction is achieved. Then, with reduced conduction losses, the generator can operate cooler and the winding resistances tend to be smaller, which reduces conduction losses even more.

The experimental results obtained from a prototype rated at 5 kW have demonstrated the system effectiveness, as an average efficiency above 90% for a wide power range has been achieved. Besides the improvement in the converter efficiency, reduced mechanical and electrical stresses in the generator are expected, which improves the overall system performance.

References

[1] Energy Information Administration. (2006, Jun.). International Energy Outlook, Washington, DC [Online]. Available: http://www.eia.doe.gov/oiaf/archive/aeo06/index.html

[2] Global Wind Energy Outlook 2006. (2006). Global Wind Energy Council, Bruxelas [Online]. Available: http://www.gwec.net/fileadmin/documents/Publications/Global_Wind_Energy_Outlook_2006.pdf

[3] S. Heier, *Grid Integration of Wind Energy Conversion Systems.* Hoboken, NJ: Wiley, 1998.

[4] T. Burton, D. Sharpe, N. Jenkins, and E. Bossanyi, *Wind Energy Handbook*. New York: Wiley, 2001.

[5] Z. Chen and J. M. Guerrero, "Editorial special issue on power electronics for wind energy conversion," *IEEE Trans. Power Electron.*, vol. 23, no. 3, pp. 1038–1040, May 2008.

[6] S. Grabic, N. Celanovic, and V.A. Katic, "Permanent magnet synchronous generator cascade for wind turbine application," *IEEE Trans. Power Electron.*, vol. 23, no. 3, pp. 1136–1142, May 2008.

[7] F. Blaabjerg, Z. Chen, and S. B. Kjaer, "Power electronics as efficient interface in dispersed power generation systems," *IEEE Trans. Power Electron.*, vol. 19, no. 5, pp. 1184–1194, Sep. 2004.

[8] J. M. Carrasco, L. G. Franquelo, J. T. Bialasiewicz, E. Galvan, R. C. P. Guisado, M. A. M. Prats, J. I. Leon, and N. Moreno-Alfonso, "Power-electronic systems for the grid integration of renewable energy sources: A survey," *IEEE Trans. Ind. Electron.*, vol. 53, no. 4, pp. 1002–1016, Jun. 2006.

[9] J. A. Baroudi, V. Dinavahi, and A. M. Knight, "A review of power converter topologies for wind generators," in *Proc. IEEE Int. Conf. Electr. Mach. Drives*, May, 2005, pp. 458–465.

[10] F. Blaabjerg, R. Teodorescu, M. Liserre, and A. V. Timbus, "Overview of control and grid synchronization for distributed power generation systems," *IEEE Trans. Ind. Electron.*, vol. 53, no. 5, pp. 1398–1409, Oct. 2006.

[11] E. Muljadi, C. P. Butterfield, and Y. H. Wan, "Axial-flux modular permanent-magnet generator with a toroidal winding for wind-turbine applications," *IEEE Trans. Ind. Appl.*, vol. 35, no. 4, pp. 831–836, Jul./Aug. 1999.

[12] Z. Chen and E. Spooner, "Voltage source inverters for high-power, variable-voltage DC power sources," *Inst. Electr. Eng. Proc.Generation, Transmiss. Distrib.*, vol. 148, no. 5, pp. 439–447, Sep. 2001.

[13] Z. Chen and E. Spooner, "Wind turbine power converters: A comparative study," in *Proc. IEE Int. Conf. PEVD1998*, London, U.K., Sep., pp. 471–476.

[14] T. F. Chan and L. L. Lai, "Permanent-magnet machines for distributed power generation: A review," in *Proc. IEEE Power Eng. Soc. Gen. Meet.*, Jun. 2007, pp. 1–6.
[15] *IEEE Recommended Practices and Requirements for Harmonic Control in Electrical Power Systems*, IEEE Standard 519, 1992, 2010.
[16] A. R. Prasad, P. D. Ziogas, and S. Manias, "An active power factor correction technique for three-phase diode rectifiers," *IEEE Trans. Power Electron.*, vol. 6, no. 1, pp. 83–92, Jan. 1991.
[17] Y. Higuchi, N. Yamamura, M. Ishida, and T. Hori, "An improvement of performance for small-scaled wind power generating system with permanent magnet type synchronous generator," in *Proc. 26th Annu. Conf. IEEE Ind. Electron. Soc. (IECON 2000*, vol. 2, pp. 1037–1043.
[18] S. H. Song, S. Kang, and N. Hahm, "Implementation and control of grid connected AC–DC–AC power converter for variable speed wind energy conversion system," in *Proc. 18th Annu. IEEE Appl. Power Electron. Conf. Expo.*, Feb. 2003, vol. 1, pp. 154–158.
[19] X. Xin and L. Hui, "Research on multiple boost converter based on MW-level wind energy conversion system," in *Proc. 8th Int. Conf. Electr. Mach. Syst.*, Sep. 2005, vol. 2, pp. 1046–1049.
[20] D. S. Oliveira, Jr., I. R. Machado, L. H. S. C. Barreto, H. M. O. Filho, R. O. Souza, and M. M. Reis, "Sistema eólico de pequeno porte para carregamento de baterias," *Brazilian J. Power Electron.*, vol. 12, pp. 97–104, Jul. 2007.
[21] H. M. Suryawanshi, M. R. Ramteke, K. L. Thakre, and V. B. Borghate, "Unity-power-factor operation of three-phase AC–DC soft switched converter based on boost active clamp topology in modular approach," *IEEE Trans. Power Electron.*, vol. 23, no. 1, pp. 229–236, Jan. 2008.
[22] I. Schiemenz and M. Stiebler, "Control of a permanent magnet synchronous generator used in a variable speed wind energy system," in *Proc. IEEE Int. Electr. Mach. Drives Conf. (IEMDC 2001*, pp. 872–877.
[23] A. B. Raju, B. G. Fernandes, and K. Chatterjee, "A UPF power conditioner with maximum power point tracker for grid connected variable speed wind energy conversion system," in *Proc. 1st Int. Conf. Power Electron. Syst. Appl.*, Nov. 2004, pp. 107–112.
[24] G. T. Kim and T. A. Lipo, "VSI-PWM rectifier/inverter system with a reduced switch count," *IEEE Trans. Ind. Appl.*, vol. 32, no. 6, pp. 1331–1337, Nov./Dec. 1996.
[25] A. B. Raju, K. Chatterjee, and B. G. Fernandes, "A simple maximum power point tracker for grid connected variable speed wind energy conversion system with reduced switch count power converters," in *Proc. IEEE 34th Annu. Power Electron. Spec. Conf. (PESC 2003)*, Jun., pp. 748–753.
[26] M. B. de Correa, C. B. Jacobina, E. R. C. da Silva, and A. M. N. Lima, "A general PWM strategy for four-switch three-phase inverters," *IEEE Trans. Power Electron.*, vol. 21, no. 6, pp. 1618–1627, Nov. 2006.
[27] C. B. Jacobina, E. C. dos Santos, E. R. C. da Silva, M. B. de Correa, A. M. N. Lima, and T. M. Oliveira, "Reduced switch count multiple three-phase AC machine drive systems," *IEEE Trans. Power Electron.*, vol. 23, no. 2, pp. 966–976, Mar. 2008.
[28] D. S. C. Oliveira, Jr., C. A Bissochi, Jr., F. Vincenzi, J. B. Vieira, Jr., V. J. Farias, and L. C. de Freitas, "Proposal of a new audio amplifier," in *Proc. IEEE Int. Power Eletron. Congr. (CIEP)*, Acapulco, Mexico, 2000, pp. 330–334.
[29] M. M. Reis, B. L. Soares, L. H. S. C. Barreto, C. E. A. Silva, R. P. T. Bascopé, and D. S. Oliveira, Jr., "A variable speed wind energy conversion system connected to the grid for small wind generator," in *Proc. 23rd Annu. IEEE Appl. Power Electron. Conf. Expo. (APEC 2008)*, Feb. 24–28, pp. 751–755.

Demercil S. Oliveira Jr. was born in Santos, São Paulo, Brazil, in 1974. He received the B.Sc. and M.Sc. degrees in electrical engineering from the Federal University of Uberlândia, Uberlândia, Brazil, in 1999 and 2001, respectively, and the Ph.D. degree from the Federal University of Santa Catarina, Florianópolis, Brazil, in 2004.

He is currently a Researcher in the Group of Power Processing and Control, Federal University of Ceará, Fortaleza, Brazil. His research interests include dc/dc conversion, soft commutation, and renewable energy applications.

Mônica Magalhães Reis received the B.Sc. and M.Sc. degrees in electrical engineering from Federal University of Ceará, Fortaleza, Brazil, in 2005 and 2008, respectively.

She is currently a Faculty member with the Federal University of Ceará. Her research interests included power electronics and renewable energy applications.

Carlos Elmano de Alencar e Silva was born in Fortaleza, Ceará, Brazil, in 1981. He received the B.Sc. and M.Sc. degrees in electrical engineering in 2004 and 2007, respectively, from the Federal University of Ceará, Fortaleza, Brazil, where he is currently working toward the Ph. D. degree.

His research interest include ac–dc conversion with high power factor, dc–ac conversion, and renewable energy applications.

Luiz Henrique Silva Colado Barreto (M'07) was born in Navirai, MS, Brazil. He received the B.Sc. degree in electrical engineering from the Universidade Federal de Mato Grosso, Cuiabá, Brazil, in 1997, and the M.Sc. and Ph.D. degrees from the Universidade Federal de Uberlândia, Uberlândia, Brazil, in 1999 and 2003, respectively.

Since June 2003, he has been with the Department of Electrical Engineering, Universidade Federal do Ceará, Fortaleza, Brazil, where he is currently a Professor of electrical engineering. His research interests include high-frequency power conversion, modeling and control of converters, power factor correction circuits, and new converters topologies, uninterruptible power system systems, and fuel cells.

Fernando L. N. Antunes (M'80) received the B.Sc. degree in electrical engineering from the Federal University of Ceará, Fortaleza, Brazil, in 1978, the B.Sc. degree in business and administration from the State University of Ceara, Fortaleza, in 1983, the M.Sc. degree from the University of São Paulo, São Paulo, Brazil, in 1980, and the Ph.D. degree from Loughborough University of Technology, Leicester, U.K., in 1991, where he was involved in the field of power electronics and machine drives.

He is currently a Senior Lecturer in the Group of Power Processing and Control, Federal University of Ceará. His research interests include multilevel converters, inverters, and their application to renewable energy.

Dr. Antunes is a Member of IEEE Power Electronics Society and the Brazilian Power Electronics Society.

Bruno L. Soares, photograph and biography not available at the time of publication.